Organic Photovoltaic Cells Based on Continuously Graded Donor–Acceptor Heterojunctions

Richa Pandey and Russell J. Holmes, *Member, IEEE*

(Invited Paper)

***Abstract*—We demonstrate enhanced organic photovoltaic cell (OPV) efficiency through the use of continuously graded donor–acceptor (D–A) heterojunctions. Device performance is a strong function of both D–A grading and overall composition ratio. The use of a tunable gradient permits an increase in the D–A interface area for high-exciton diffusion efficiency relative to a planar heterojunction, while also improving the charge collection efficiency relative to a uniform mixture. Using the archetypical D–A pair of copper phthalocyanine and C_{60}, a power conversion efficiency of $\eta_P = (2.1 \pm 0.1)\%$ is realized under 100 mW/cm^2 simulated AM1.5G solar illumination for a graded heterojunction. This represents an improvement in η_P of $\sim$60% relative to a planar heterojunction OPV and $\sim$20% compared to a uniformly mixed heterojunction OPV.**

***Index Terms*—Excitons, molecular electronics, organic compounds, photovoltaic cells, semiconductor heterojunctions.**

I. Introduction

SINCE the first demonstration of an efficient organic photovoltaic cell (OPV) by Tang [1], refinements in both device design and materials selection have led to significant improvements in performance [2]–[4]. In particular, previous work has emphasized the importance of film morphology in realizing high-power conversion efficiency (η_P) [3]–[5]. In this paper, OPV morphology is engineered through the use of continuously graded film compositions. The highly tunable gradient permits fine control over device performance, enabling improvements in efficiency.

In an organic semiconductor, photon absorption leads to the formation of tightly bound, mobile excitons. Excitons diffuse to a donor–acceptor (D–A) heterojunction and are dissociated if the interface energy-level offset exceeds the exciton binding energy [6], [7]. Following dissociation, charge carriers are collected at their respective electrodes [8]. The fraction of photogenerated excitons that reach the D–A interface is referred to as the exciton diffusion efficiency. Similarly, the charge collection efficiency is defined as the fraction of dissociated charge carriers that reach the electrodes. In a planar heterojunction OPV, device performance is limited by a low-absorption efficiency since the active layer thickness is comparable to the exciton diffusion length (L_D), which is much smaller than the optical absorption length [6]. The competition between the requirements for efficient optical absorption and exciton diffusion is known as the "exciton bottleneck."

Multiple approaches have been developed to overcome the exciton bottleneck and realize efficient photoconversion in OPVs. The use of long-lived phosphorescent materials has enabled larger L_D than is typically obtained in fluorescent organic materials [9]–[13]. Of particular note is the use of C_{60} as an acceptor, permitting thicker active layers and enhanced device performance [9], [10]. To date, the most significant improvements in device performance have come from advances in the control of film composition and morphology. Architectures including mixed [14]–[16], hybrid planar-mixed [17], [18], nanocrystalline [4], [19], and bulk [2], [10], [20], [21] heterojunctions have attempted to overcome the short L_D by increasing the D–A interface area thereby improving the exciton diffusion efficiency.

The use of a uniformly mixed D–A heterojunction is attractive as it permits efficient exciton diffusion by extending the dissociating interface throughout the film [14]–[16]. Unfortunately, the charge carrier mobility is typically reduced in these structures, especially in mixtures of small molecules, potentially leading to a lower charge collection efficiency [22], [23]. A promising alternative to the use of uniform mixtures are graded D–A heterojunctions (GHJs). Previous work on GHJs in OPVs has focused on the use of multistepped structures that comprise thin, uniformly mixed layers of varying D–A composition to simulate a gradient [14], [24], [25]. In these initial investigations, there is no discussion of GHJ performance as a function of the D–A composition ratio or active layer thickness. In addition, no evidence is presented that confirms an enhancement in the charge collection efficiency relative to a uniformly mixed architecture. In order to conclusively demonstrate the merits of the GHJ architecture, this study utilizes a continuous, D–A concentration gradient throughout the active layer. The GHJ has a larger D–A interface area than a planar heterojunction, and for an optimized composition profile, maintains a high-charge collection efficiency relative to a uniform mixture. Consequently, this architecture allows for significant optimization and tuning of the exciton diffusion and charge collection efficiencies through modifications of the composition profile.

Manuscript received February 3, 2010; revised April 1, 2010; accepted April 19, 2010. Date of publication June 21, 2010; date of current version December 3, 2010. This work was supported in part by the National Science Foundation (NSF) under Award CBET-0946723 and in part by the NSF Materials Research Science and Engineering Centers Program under Awards DMR-0212302 and DMR-0819885. The work of R. J. Holmes was supported in part by 3M Company under a Non-Tenured Faculty Grant.

The authors are with the Department of Chemical Engineering and Materials Science, University of Minnesota, Minneapolis, MN 55455 USA (e-mail: rholmes@umn.edu).

Digital Object Identifier 10.1109/JSTQE.2010.2049256

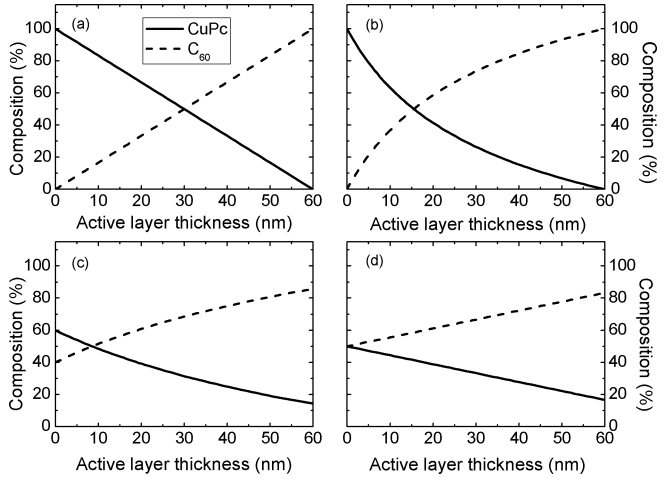

Fig. 1. Composition profile in (a) a ZEP (1:1) CuPc:C_{60} gradient, (b) a ZEP (1:2) CuPc:C_{60} gradient, (c) a NZEP gradient, and (d) a C_{60}-favorable gradient. The zero of thickness is referenced at the anode–organic interface.

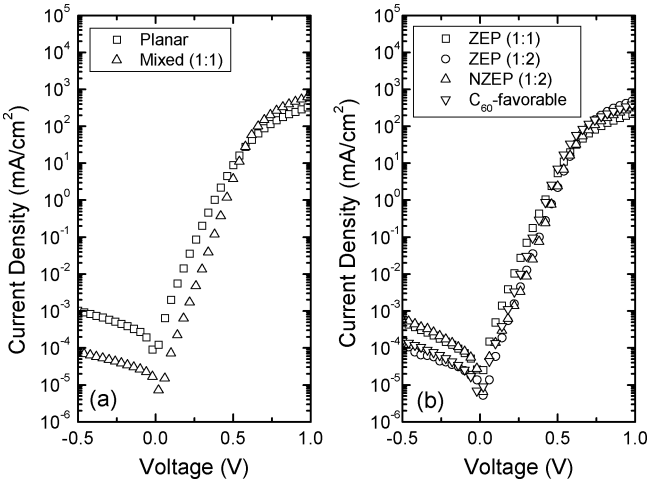

Fig. 2. Dark current–voltage characteristics for a variety of optimized CuPc:C_{60} OPV architectures. (a) Planar and uniformly mixed (1:1) heterojunction OPVs. (b) GHJ OPVs with active layers consisting of either a ZEP (1:1), ZEP (1:2), NZEP, or C_{60}-favorable gradient. The active layer thickness for each device is shown in Table I.

II. Experiment

In this work, OPVs were fabricated on indium-tin-oxide-coated glass substrates with a sheet resistance of 15 Ω/□ and a thickness of 150 nm. Substrates were degreased with detergent and solvents and then cleaned by exposure to a UV-ozone ambient. Organic layers were deposited by high-vacuum thermal sublimation at a pressure of 8×10^{-7} Torr. OPVs containing GHJs were constructed using copper phthalocyanine (CuPc) and C_{60} as the donor and acceptor materials, respectively. For this study, CuPc and C_{60} were obtained from Acros Organics (∼95% purity) and MER Corporation (∼99%), respectively. All materials were used as received without further purification.

In order to construct films with graded composition profiles, donor and acceptor deposition rates were ramped linearly with time and monitored using two quartz crystal monitors. The concentration gradients of interest are shown in Fig. 1. The gradients of Fig. 1(a) and (b) are henceforth, referred to as "zero endpoint" (ZEP) gradients. In Fig. 1(a), the ratio of CuPc to C_{60} is 1:1 (by wt.), while in Fig. 1(b) the D–A ratio is 1:2. The ZEP (1:1) gradient in Fig. 1(a) was constructed by varying the growth rates (*R*) of CuPc and C_{60} according to $R_{\mathrm{CuPc}} = 0.2$ nm/s→0 nm/s and $R_{\mathrm{C60}} = 0$ nm/s→0.2 nm/s, respectively. The gradient of Fig. 1(b) was constructed by varying the growth rates according to $R_{\mathrm{CuPc}} = 0.1$ nm/s→0 nm/s and $R_{\mathrm{C60}} = 0$ nm/s→0.2 nm/s, respectively. The non-zero endpoint (NZEP) gradient of Fig. 1(c) was constructed by varying the growth rates according to $R_{\mathrm{CuPc}} = 0.075$ nm/s→0.025 nm/s and $R_{\mathrm{C60}} = 0.05$ nm/s→0.15 nm/s, respectively. The NZEP gradient has a 1:2 ratio of CuPc to C_{60}. A modified version of the NZEP is the "C_{60}-favorable" gradient, as shown in Fig. 1(d), which maintains a composition of ≥50 wt.% C_{60} throughout the GHJ. The C_{60}-favorable gradient was constructed by varying the growth rates according to $R_{\mathrm{CuPc}} = 0.1$ nm/s→0.033 nm/s and $R_{\mathrm{C60}} = 0.1$ nm/s→0.167 nm/s, respectively. For the aforementioned gradients, the composition endpoints are kept fixed when varying the active layer thickness. This permits a constant injection barrier to be maintained at the electrode–organic interfaces. Given the use of a dry, evaporative deposition process, negligible molecular diffusion is expected to occur in these films [20]. A 10-nm-thick layer of bathocuproine (BCP) was grown on top of the active layers in all of the OPV architectures to serve as an exciton-blocking layer [9], [22], [26]. The organic multilayer is capped with an Al cathode, which is deposited through a shadow mask defining devices 1 mm in diameter. Planar heterojunction OPVs used as control devices consisted of a 20-nm-thick layer of CuPc and a 40-nm-thick layer of C_{60}.

Photovoltaic characterization was carried out in air ambient at 25 °C immediately after growth under simulated AM1.5G solar irradiance (150 W Oriel solar simulator). Current–voltage characteristics were measured as a function of optical illumination using an Agilent Technologies 4155C semiconductor parameter analyzer. A Newport 818P-010–12 high-power detector was used to measure the incident optical power during each testing session. The external quantum efficiency (η_{EQE}) was measured using monochromatic light chopped at a frequency of 200 Hz. Photocurrent measurements were made at each wavelength, using a lock-in amplifier. The incident optical power was measured as a function of wavelength, using a Newport 818-UV photodetector.

III. Results

Fig. 2 compares the dark current–voltage characteristics for planar, uniformly mixed, and GHJ OPVs. Figs. 3 and 4 show operating parameters for devices with ZEP (1:1), ZEP (1:2), and NZEP GHJs as a function of active layer thickness under simulated AM1.5G solar illumination at 100 mW/cm^2. The short-circuit current density (J_{SC}) increases with thickness for all three gradients [Fig. 3(a)]. The J_{SC} values are lower for the ZEP architectures relative to the NZEP architecture. The open-circuit voltage (V_{OC}) does not depend strongly on GHJ type

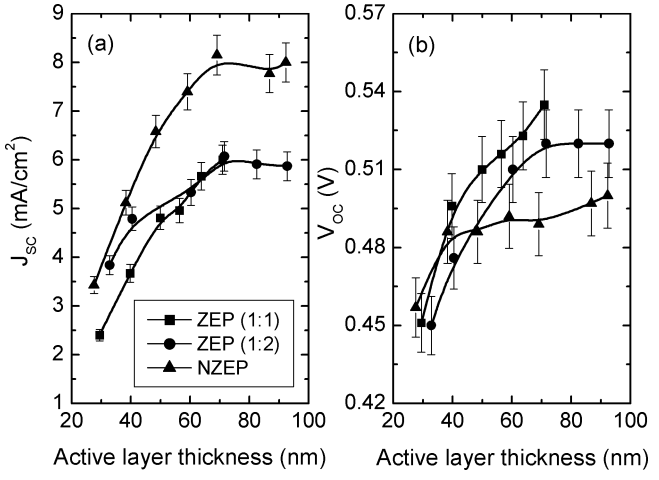

Fig. 3. (a) Short-circuit current density ($J_{\rm SC}$), and (b) open-circuit voltage ($V_{\rm OC}$) for devices containing ZEP (1:1) CuPc:C_{60}, ZEP (1:2) CuPc:C_{60}, and NZEP graded composition profiles under illumination at 100 mW/cm^2 as a function of active layer thickness.

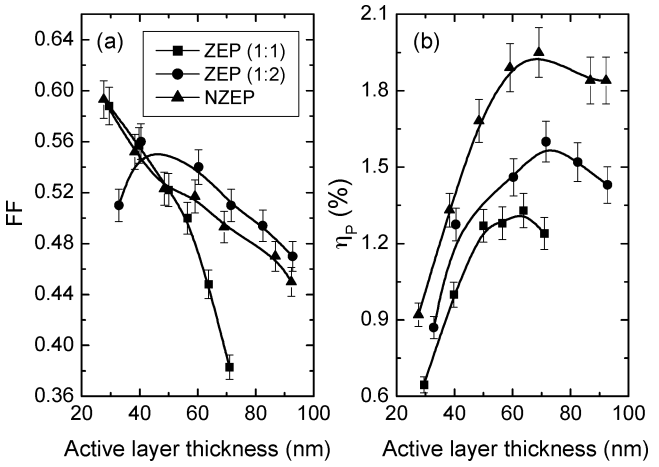

Fig. 4. (a) Fill factor (FF) and (b) power conversion efficiency (η_P) for devices containing ZEP (1:1) CuPc:C_{60}, ZEP (1:2) CuPc:C_{60}, and NZEP graded composition profiles under illumination at 100 mW/cm^2 as a function of active layer thickness.

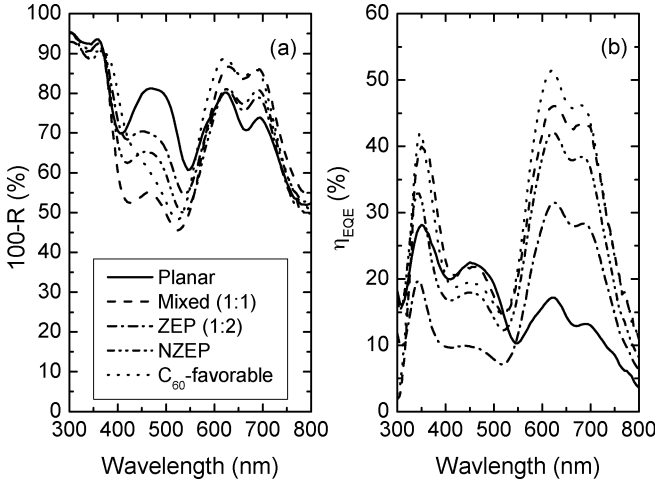

Fig. 5. (a) Relative absorption efficiency (100%-Reflectivity) and (b) external quantum efficiency ($\eta_{\rm EQE}$) spectra for a planar heterojunction OPV, a uniformly mixed heterojunction OPV containing 1:1 CuPc:C_{60} (73 nm), and GHJ OPVs with active layers consisting of either a ZEP (1:2) CuPc:C_{60} gradient (72 nm), a NZEP gradient (69 nm), or a C_{60}-favorable gradient (71 nm).

[Fig. 3(b)], and in general increases with active layer thickness. The fill factor (FF) for all three GHJs decreases with increasing thickness [Fig. 4(a)]. The FF increases significantly upon changing the CuPc:C_{60} ratio from 1:1 to 1:2. This high FF is also observed for the NZEP gradient, which is characterized by a 1:2 ratio of CuPc to C_{60}. Together these parameters result in a η_P of $(2.0 \pm 0.1)\%$ for the NZEP graded architecture at an active layer thickness of 69 nm [Fig. 4(b)].

The spectral response of GHJ OPVs was compared to that of conventional planar and uniformly mixed device architectures. The relative absorption efficiency for each OPV was estimated by measuring normal incidence device transmissivity and reflectivity (R) at an angle of 15° from normal. Since transmissivity through the opaque metal cathode is $\sim 10^{-4}$, the relative absorption efficiency can be approximated as 100–R (%). It is important to note that while useful for comparisons of the relative absorption efficiency, this technique is not suitable for the calculation of the absolute absorption efficiency as it also includes absorption in the anode and cathode layers. Fig. 5 shows the relative absorption and $\eta_{\rm EQE}$ spectra for planar, mixed (1:1), and a variety of GHJ OPVs. The active layer thicknesses for the mixed (1:1), ZEP (1:2), NZEP, and C_{60}-favorable GHJ OPVs are 73, 72, 69, and 71 nm, respectively. In all cases, the photoresponse occurring at wavelengths $\lambda \geq 525$ nm originates from absorption in CuPc [Fig. 5(a)]. The device response observed at shorter wavelengths corresponds mainly to absorption in C_{60}. The use of graded and mixed heterojunctions drastically improves the $\eta_{\rm EQE}$ of CuPc relative to a planar device [Fig. 5(b)]. Both the ZEP (1:2) and NZEP architectures show a much lower C_{60} response than the uniformly mixed heterojunction. In order to further improve the C_{60} response, a C_{60}-favorable gradient was constructed [Fig. 1(d)]. This gradient is characterized by a C_{60} composition of $\geq$50 wt.% throughout the active layer. An optimum active layer thickness of 71 nm was experimentally determined for this gradient. An increase in $\eta_{\rm EQE}$ is realized for the C_{60}-favorable gradient relative to both the NZEP gradient and a uniformly mixed device.

Figs. 6 and 7 show OPV parameters for devices containing either a C_{60}-favorable gradient or a uniform mixture with 1:1 or 1:2 CuPc:C_{60} as a function of active layer thickness under simulated AM1.5G solar illumination at 100 mW/cm^2. At an optimum layer thickness of 71 nm, the highest $J_{\rm SC}$ is realized with the C_{60}-favorable gradient while the $J_{\rm SC}$ values for mixed 1:2 devices were lowest [Fig. 6(a)]. The $V_{\rm OC}$ increases with thickness, as noted previously [Fig. 6(b)]. While the FF for OPVs containing a mixed (1:1) heterojunction decreases steeply with increasing active layer thickness, the FFs for the mixed (1:2) and C_{60}-favorable GHJs show a much weaker dependence on active layer thickness [Fig. 7(a)]. These parameters lead to an η_P of $(2.1 \pm 0.1)\%$ for the C_{60}-favorable gradient at a thickness

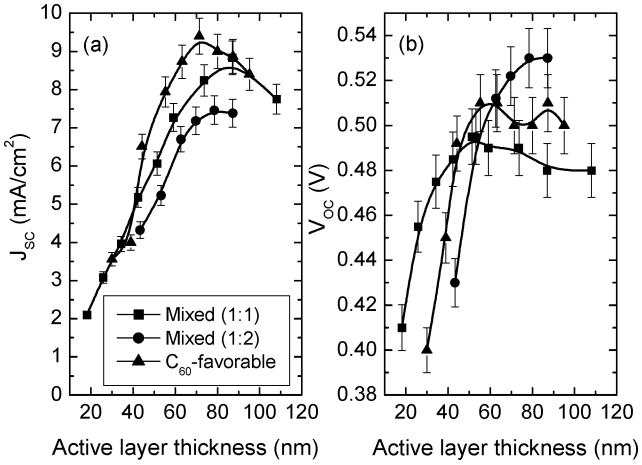

Fig. 6. (a) Short-circuit current density ($J_{\rm SC}$) and (b) open-circuit voltage ($V_{\rm OC}$) for devices containing a mixed heterojunction with either 1:1 or 1:2 CuPc:C_{60}, or a C_{60}-favorable GHJ under illumination at 100 mW/cm^2 as a function of active layer thickness.

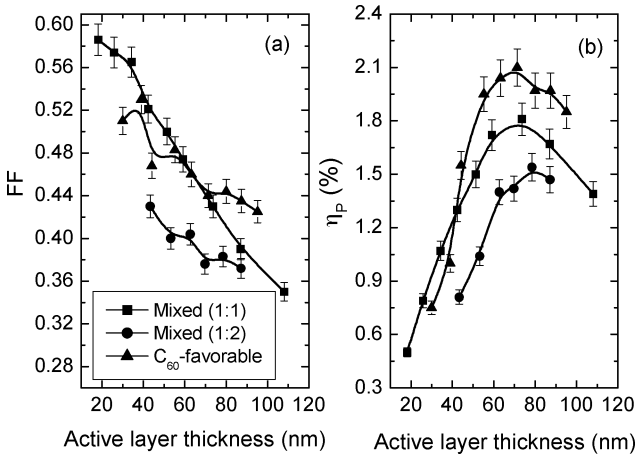

Fig. 7. (a) Fill factor (FF) and (b) power conversion efficiency (η_P) for devices containing a mixed heterojunction with either 1:1 or 1:2 CuPc:C_{60}, or a C_{60}-favorable GHJ under illumination at 100 mW/cm^2 as a function of active layer thickness.

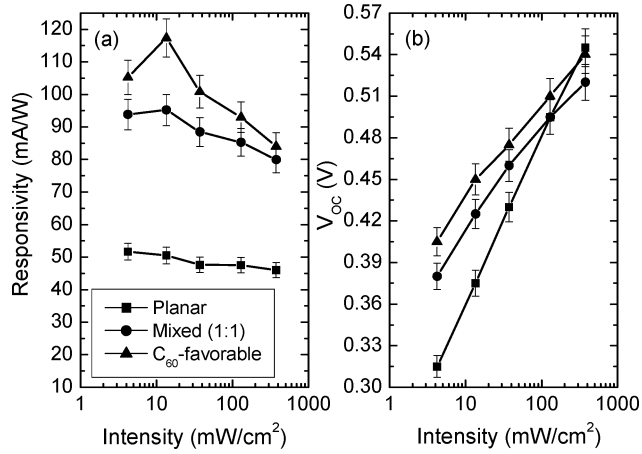

Fig. 8. (a) Responsivity and (b) open-circuit voltage ($V_{\rm OC}$) for CuPc:C_{60} OPVs with planar (20 nm CuPc/40 nm C_{60}), mixed (1:1) (73 nm), or C_{60}-favorable graded (71 nm) architectures as a function of illumination intensity.

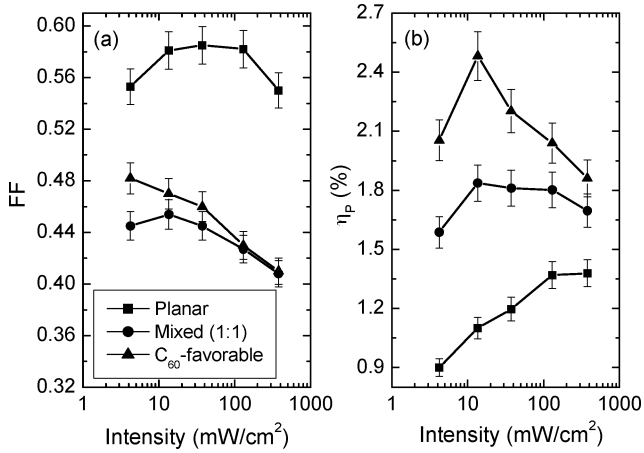

Fig. 9. (a) Fill factor (FF) and (b) power conversion efficiency (η_P) for CuPc:C_{60} OPVs with planar (20 nm CuPc/40 nm C_{60}), mixed (1:1) (73 nm), or C_{60}-favorable graded (71 nm) architectures as a function of illumination intensity.

of 71 nm and (1.8 $\pm$ 0.1)% for the mixed (1:1) heterojunction at a thickness of 73 nm [Fig. 7(b)].

Figs. 8 and 9 compare the performance of a C_{60}-favorable GHJ OPV with that of optimized planar and mixed (1:1) heterojunction OPVs. The peak responsivity for the C_{60}-favorable gradient is (117 $\pm$ 6) mA/W at low-illumination intensity and decreases to (95 $\pm$ 5) mA/W at 100 mW/cm^2 [Fig. 8(a)]. The $V_{\rm OC}$ increases linearly with the logarithm of illumination intensity for all three devices [Fig. 8(b)]. Overall, a peak η_P of (2.5 $\pm$ 0.1)% is obtained for the C_{60}-favorable architecture at 13.5 mW/cm^2, falling to (2.1 $\pm$ 0.1)% at 100 mW/cm^2, compared to (1.8 $\pm$ 0.1)% for a uniformly mixed device, and (1.4 $\pm$ 0.1)% for a planar device [Fig. 9(b)]. The operating parameters obtained for planar and uniformly mixed OPVs are consistent with those published elsewhere for comparable active materials and device architectures [4], [14], [19], [27], [28].

IV. Discussion

A. Dark Current Characteristics

The dark current–voltage characteristics for GHJ OPVs were compared to those of conventional planar and mixed architectures (see Fig. 2). For this comparison, the active layer of the mixture was 73 nm thick with a 1:1 ratio of CuPc to C_{60}. The dark current in an OPV is often modeled using the Shockley equation [29]–[34].

$$J = J_s \left\{ \exp\left(\frac{e(V - JR_s)}{nkT} \right) - 1 \right\} \tag{1}$$

where J is the current density, J_s is the reverse-bias saturation current density, e is the electron charge, R_s is the series resistance, n is the ideality factor, k is the Boltzmann constant, and T is the temperature. The dark current–voltage characteristics were fit, using (1), and the fit parameters are shown in Table I.

TABLE I
DARK CURRENT CHARACTERISTICS FOR VARIOUS DEVICE ARCHITECTURES

Structure	Thickness (nm)	n	J_s (A/cm^2)	R_s (Ω cm^2)
Planar (20 nm CuPc/40 nm C_{60})	60	1.95	$5.0\text{x}10^{-7}$	1.02
Mixed (1:1 CuPc:C_{60})	73	1.40	$4.0\text{x}10^{-9}$	0.48
Zero Endpoint Graded (1:1)	29	1.87	$1.9\text{x}10^{-7}$	0.44
	50	1.70	$3.0\text{x}10^{-8}$	0.76
	71	1.67	$6.0\text{x}10^{-9}$	1.52
Zero Endpoint Graded (1:2)	60	1.47	$4.8\text{x}10^{-9}$	0.57
Non-zero Endpoint Graded (1:2)	69	1.51	$6.8\text{x}10^{-9}$	0.93
C_{60}-Favorable Graded (1:2)	71	1.41	$8.8\text{x}10^{-9}$	0.88

The ideality factor is reduced from (1.95 ± 0.02) for a planar heterojunction to (1.40 ± 0.02) for a mixed heterojunction OPV. For a ZEP (1:1) GHJ OPV, the ideality factor decreases with increasing thickness, with a value of (1.67 ± 0.01) realized at an optimum active layer thickness of 71 nm. These values indicate that the dark current in the planar architecture is dominated by electron–hole recombination. In the more disordered graded and mixed heterojunction OPVs, the reduced ideality factor suggests an additional contribution to the dark current from charge carrier diffusion [35]. Lower J_s values are obtained for mixed and GHJ OPVs compared to a planar heterojunction OPV due to a reduction in the charge carrier mobilities as a result of molecular intermixing [17], [23], [36]. The J_s value is also observed to decrease from $(1.9 \pm 0.4) \times 10^{-7}$ A/cm^2 to $(6.0 \pm 1.3) \times 10^{-9}$ A/cm^2 as the thickness increases from 29 to 71 nm, suggesting that the charge collection efficiency could be reduced for thick active layers. Similar trends in J_s are also observed for the other graded and mixed heterojunction OPVs studied in this study. Comparable R_s values are obtained for the various device architectures, suggesting that for these thicknesses, R_s may be determined by the anode–organic interface [37].

B. Impact of Gradient on Performance

Figs. 3 and 4 show a strong correlation between GHJ OPV performance and active layer thickness. For the ZEP (1:1), ZEP (1:2), and NZEP GHJs, the $J_{\rm SC}$ increases with thickness as a result of increasing optical absorption [Fig. 3(a)]. The low $J_{\rm SC}$ values observed for the ZEP architectures result from a low-exciton diffusion efficiency at the edges of the GHJ. The exciton diffusion efficiency is improved by adjusting the ZEP gradient to the NZEP architecture, increasing the D–A interface area near the anode/GHJ and GHJ/BCP interfaces. The improvement in exciton diffusion efficiency for the NZEP gradient results in an increase in $J_{\rm SC}$ relative to the ZEP GHJs. The $V_{\rm OC}$ increases with thickness as a result of increased photocurrent and reduced dark current with increasing active layer thickness [see Fig. 3(b)] [38]. The FF for all three GHJs decreases with increasing thickness [see Fig. 4(a)], reflecting a reduction in the charge collection efficiency, which is further supported by the observed reduction in J_s. The increase in the GHJ FF upon changing the CuPc:C_{60} ratio from 1:1 to 1:2 indicates that the charge collection is initially limited by electron transport [39]. This observation is further supported by the increase in FF observed for the NZEP gradient, which contains 1:2 CuPc:C_{60}. The large $J_{\rm SC}$ and FF obtained for the NZEP GHJ lead to the highest η_P being observed for this gradient [see Fig. 4(b)].

Fig. 5 compares the spectral response of planar, mixed (1:1), and a variety of GHJ OPVs. The use of graded and mixed heterojunctions leads to a significant enhancement in the response from CuPc relative to a planar device due to the short L_D in this material [6]. The lower $\eta_{\rm EQE}$ observed for C_{60} in the ZEP (1:2) and NZEP GHJs compared to a mixed heterojunction device suggests that the product of the exciton diffusion and charge collection efficiencies for C_{60} is smaller in these unoptimized gradients than in the mixture. As mentioned previously, charge collection in the GHJ is limited by electron transport, and further improvements in device performance were realized by addressing this specific deficiency. Previous work examining the carrier mobility in uniform mixtures of CuPc and C_{60} has shown that the electron mobility in C_{60} decreases if it comprises less than 50 wt.% of the mixture [40]. As such, the NZEP gradient was modified to ensure that the C_{60} component of the GHJ remains $\geq$50 wt.% throughout the film. An increase in $\eta_{\rm EQE}$ is realized using the C_{60}-favorable gradient, which relative to the NZEP gradient has optimized exciton diffusion and charge collection efficiencies for both active materials. Compared to a uniformly mixed OPV, the C_{60}-favorable gradient shows a $\sim$25% increase in the CuPc response at $\lambda\sim$620 nm. Since these structures have comparable absorption efficiencies for CuPc [see Fig. 5(a)], this improvement implies that the C_{60}-favorable architecture has a larger internal quantum efficiency than the uniformly mixed OPV. Given the high-diffusion efficiency characteristic of a mixture, this result also indicates that the charge collection efficiency is larger in the C_{60}-favorable gradient than in a uniform mixture.

Figs. 6 and 7 compare the performance of a C_{60}-favorable gradient with mixed (1:1) and mixed (1:2) OPVs as a function of active layer thickness. The C_{60}-favorable gradient shows the largest $J_{\rm SC}$ implying that this gradient has optimized exciton diffusion and charge collection efficiencies relative to both uniformly mixed architectures [see Fig. 6(a)]. The large FF observed for the C_{60}-favorable gradient relative to the mixed (1:2) heterojunction confirms that the FF is impacted favorably by the graded composition of the active layer [see Fig. 7(a)]. In addition, the large FF observed at high thickness for the C_{60}-favorable gradient relative to the mixed (1:1) heterojunction suggests that the charge transport is significantly improved in GHJ OPVs with thick active layers. Consequently, the highest

η_P is observed for the C_{60}-favorable gradient, with the improvement at small thicknesses originating from an increase in J_{SC}, and the improvement at large thicknesses coming from an increased FF.

Figs. 8 and 9 compare the performance of a C_{60}-favorable GHJ OPV to that of optimized planar and mixed heterojunctions as a function of illumination intensity. The responsivity for all three device architectures decreases with illumination intensity due to a reduction in the charge collection efficiency [see Fig. 8(a)]. The slope of V_{OC} versus illumination intensity varies depending on the device architecture, reflecting a difference in the ideality factor [see Fig. 8(b)] [36]. The disordered graded and mixed heterojunctions have lower FFs relative to the planar heterojunction due to a reduction in the charge collection efficiency [see Fig. 9(a)]. However, the reduction in FF is more than offset by an increase in responsivity for the C_{60}-favorable gradient, resulting in the highest η_P being observed for this architecture [see Fig. 9(b)].

V. Conclusion

In summary, we have demonstrated that continuously graded D–A heterojunctions offer an attractive approach to engineering morphology in small molecule OPVs. All of the GHJ OPVs studied in this study show a higher η_P at optimum active layer thickness than a planar heterojunction OPV. The NZEP and C_{60}-favorable GHJs also have higher η_P than the optimized mixed heterojunctions investigated. For thick active layers, the FF for these GHJs is $\sim$20% larger than that of a uniformly mixed (1:1) heterojunction, suggesting improved charge transport in the GHJs. This study shows conclusively that the large D–A interface area in a GHJ increases the exciton diffusion efficiency relative to a planar heterojunction, while also improving charge transport relative to a uniformly mixed OPV. Ultimately, the true potential of this approach to OPV design is the ability to tune the exciton diffusion and charge collection efficiencies based on the choice of D–A concentration gradient in order to maximize overall efficiency.

References

[1] C. W. Tang, "Two-layer organic photovoltaic cell," *Appl. Phys. Lett.*, vol. 48, pp. 183–185, 1986.

[2] S. H. Park, A. Roy, S. Beaupré, S. Cho, N. Coates, J. S. Moon, D. Moses, M. Leclerc, K. Lee, and A. J. Heeger, "Bulk heterojunction solar cells with internal quantum efficiency approaching 100%," *Nature Photon.*, vol. 3, pp. 297–302, 2009.

[3] G. Li, V. Shrotriya, J. Huang, Y. Yao, T. Moriarty, K. Emery, and Y. Yang, "High-efficiency solution processable polymer photovoltaic cells by self-organization of polymer blends," *Nature Mater.*, vol. 4, pp. 864–868, 2005.

[4] F. Yang, K. Sun, and S. R. Forrest, "Efficient solar cells using all-organic nanocrystalline networks," *Adv. Mater.*, vol. 19, pp. 4166–4171, 2007.

[5] W. Ma, C. Yang, X. Gong, K. Lee, and A. J. Heeger, "Thermally stable, efficient polymer solar cells with nanoscale control of the interpenetrating network morphology," *Adv. Func. Mater.*, vol. 15, pp. 1617–1622, 2005.

[6] P. Peumans, A. Yakimov, and S. R. Forrest, "Small molecular weight organic thin-film photodetectors and solar cells," *J. Appl. Phys.*, vol. 93, pp. 3693–3723, 2003.

[7] M. Muntwiler, Q. Yang, W. A. Tisdale, and X. Y. Zhu, "Coulomb barrier for charge separation at an organic semiconductor interface," *Phys. Rev. Lett.*, vol. 101, pp. 196403-1–196403-4, 2008.

[8] B. A. Gregg and M. C. Hanna, "Comparing organic to inorganic photovoltaic cells: Theory, experiment and simulation," *J. Appl. Phys.*, vol. 93, pp. 3605–3613, 2003.

[9] P. Peumans and S. R. Forrest, "Very-high efficiency double-heterostructure copper phthalocyanine/C60 photovoltaic cells," *Appl. Phys. Lett.*, vol. 79, pp. 126–128, 2001.

[10] G. Yu, J. Gao, J. C. Hummelen, F. Wudl, and A. J. Heeger, "Polymer photovoltaic cells: Enhanced efficiencies via a network of internal donor-acceptor heterojunctions," *Science*, vol. 270, pp. 1789–1791, 1995.

[11] Y. Shao and Y. Yang, "Efficient organic heterojunction photovoltaic cells based on triplet materials," *Adv. Mater.*, vol. 17, pp. 2841–2844, 2005.

[12] W. A. Luhman and R. J. Holmes, "Enhanced exciton diffusion in an organic photovoltaic cell by energy transfer using a phosphorescent sensitizer," *Appl. Phys. Lett.*, vol. 94, pp. 153304-1–153304-3, 2009.

[13] B. P. Rand, S. Schols, D. Cheyns, H. Gommans, C. Girotto, J. Genoe, P. Heremans, and J. Poortmans, "Organic solar cells with sensitized phosphorescent absorbing layers," *Org. Electron.*, vol. 10, pp. 1015–1019, 2009.

[14] P. Sullivan, S. Heutz, S. M. Schultes, and T. S. Jones, "Influence of codeposition on the performance of CuPc-C60 heterojunction photovoltaic devices," *Appl. Phys. Lett.*, vol. 84, pp. 1210–1212, 2004.

[15] S. Uchida, J. Xue, B. P. Rand, and S. R. Forrest, "Organic small molecule solar cells with a homogeneously mixed copper phthalocyanine: C60 active layer," *Appl. Phys. Lett.*, vol. 84, pp. 4218–4220, 2004.

[16] M. Hiramoto, H. Fujiwara, and M. Yokoyama, "Three-layered organic solar cell with a photoactive interlayer of codeposited pigments," *Appl. Phys. Lett.*, vol. 58, pp. 1062–1064, 1991.

[17] J. Xue, B. P. Rand, S. Uchida, and S. R. Forrest, "A hybrid planar-mixed molecular heterojunction photovoltaic cell," *Adv. Mater.*, vol. 17, pp. 66–71, 2005.

[18] J. Drechsel, B. Mannig, D. Gebeyehu, M. Pfeiffer, K. Leo, and H. Hoppe, "MIP-type organic solar cells incorporating phthalocyanine/fullerene mixed layers and doped wide-gap transport layers," *Org. Electron.*, vol. 5, pp. 175–186, 2004.

[19] Z. R. Hong, B. Maennig, R. Lessmann, M. Pfeiffer, K. Leo, and P. Simon, "Improved efficiency of zinc phthalocyanine/C_{60} based photovoltaic cells via nanoscale interface modification," *Appl. Phys. Lett.*, vol. 90, pp. 203505-1–203505-3, 2007.

[20] P. Peumans, S. Uchida, and S. R. Forrest, "Efficient bulk heterojunction photovoltaic cells using small-molecular-weight organic thin films," *Nature*, vol. 425, pp. 158–162, 2003.

[21] T. Tsuzuki, Y. Shirota, J. Rostalski, and D. Meissner, "The effect of fullerene doping on photoelectric conversion using titanyl phthalocyanine and a perylene pigment," *Solar Energy Mater. Solar Cells*, vol. 61, pp. 1–8, 2000.

[22] B. P. Rand, J. Li, J. Xue, R. J. Holmes, M. E. Thompson, and S. R. Forrest, "Organic double-heterostructure photovoltaic cells employing thick Tris(acetylacetonato)ruthenium(III) exciton-blocking layers," *Adv. Mater.*, vol. 17, pp. 2714–2718, 2005.

[23] M. Bronner, A. Opitz, and W. Brütting, "Ambipolar charge carrier transport in organic semiconductor blends of phthalocyanine and fullerene," *Phys. Stat. Sol. (a)*, vol. 205, pp. 549–563, 2008.

[24] B. Pradhan and A. J. Pal, "Organic photovoltaic devices: Concentration gradient of donor and acceptor materials in the molecular scale," *Synth. Met.*, vol. 155, pp. 555–559, 2005.

[25] L. Chen, Y. Tang, X. Fan, C. Zhang, Z. Chu, D. Wang, and D. Zou, "Improvement of the efficiency of CuPc/C60-based photovoltaic cells using a multistepped structure," *Org. Electron.*, vol. 10, pp. 724–728, 2009.

[26] M. Vogel, S. Doka, Ch. Breyer, M. Ch. Lux-Steiner, and K. Fostiropoulos, "On the function of a bathocuproine buffer layer in organic photovoltaic cells," *Appl. Phys. Lett.*, vol. 89, pp. 163501-1–163501-3, 2006.

[27] K. Fostiropoulos, M. Vogel, B. Mertesacker, and A. Weidinger, "Preparation and Investigation of Phthalocyanine/C60 Solar Cells," *Proc. SPIE*, vol. 4801, pp. 1–6, 2003.

[28] K. L. Mutolo, E. I. Mayo, B. P. Rand, S. R. Forrest, and M. E. Thompson, "Enhanced open-circuit voltage in subphthalocyanine/C60 organic photovoltaic cells," *J. Amer. Chem. Soc.*, vol. 128, pp. 8108–8109, 2006.

[29] S. M. Sze, *Physics of Semiconductor Devices*. New York: Wiley, 1981.

[30] P. Schilinsky, C. Waldauf, and C. J. Brabec, "Performance analysis of printed bulk heterojunction solar cells," *Adv. Func. Mater.*, vol. 16, pp. 1669–1672, 2006.

[31] P. Schilinsky, C. Waldauf, J. Hauch, and C. J. Brabec, "Simulation of light intensity dependent current characteristics of polymer solar cells," *J. Appl. Phys.*, vol. 95, pp. 2816–2819, 2004.

[32] S. Yoo, B. Domercq, and B. Kippelen, "Intensity-dependent equivalent circuit parameters of organic solar cells based on pentacene and C_{60}," *J. Appl. Phys.*, vol. 97, pp. 103706-1–103706-9, 2005.
[33] M. D. Perez, C. Borek, S. R. Forrest, and M. E. Thompson, "Molecular and morphological influences on the open circuit voltages of organic photovoltaic devices," *J. Amer. Chem. Soc.*, vol. 131, pp. 9281–9286, 2009.
[34] J. D. Servaites, S. Yeganeh, T. J. Marks, and M. A. Ratner, "Efficiency enhancement in organic photovoltaic cells: Consequences of optimizing series resistance," *Adv. Func. Mater.*, vol. 20, pp. 97–104, 2010.
[35] D. A. Neaman, *Semiconductor Physics and Devices.*. New York: McGraw-Hill, 2007.
[36] J. Xue, B. P. Rand, S. Uchida, and S. R. Forrest, "Mixed donor-acceptor molecular heterojunctions for photovoltaic applications. II. Device performance," *J. Appl. Phys.*, vol. 98, pp. 124903-1–124903-9, 2005.
[37] J. Dai, X. Jiang, H. Wang, and D. Yan, "Organic photovoltaic cell employing organic heterojunction as buffer layer," *Thin Solid Films*, vol. 516, pp. 3320–3323, 2008.
[38] N. Li, B. E. Lassiter, R. R. Lunt, G. Wei, and S. R. Forrest, "Open circuit voltage enhancement due to reduced dark current in small molecule photovoltaic cells," *Appl. Phys. Lett.*, vol. 94, pp. 023307-1–023307-3, 2009.
[39] D. Gebeyehu, B. Maennig, J. Drechsel, K. Leo, and M. Pfeiffer, "Bulk-heterojunction photovoltaic devices based on donor—acceptor organic small molecule blends," *Solar Energy Mater. Solar Cells*, vol. 79, pp. 81–92, 2003.
[40] B. P. Rand, J. Xue, S. Uchida, and S. R. Forrest, "Mixed donor-acceptor molecular heterojunctions for photovoltaic applications. I. Material properties," *J. Appl. Phys.*, vol. 98, pp. 124902-1–124902-7, 2005.

Richa Pandey received the B.Tech. degree in chemical engineering from the Indian Institute of Technology, Kanpur, India, in 2007. She is currently working toward the Ph.D. degree in chemical engineering at the University of Minnesota, Minneapolis.

During Summer 2006, she completed an internship with Reliance Industries Ltd., India, where she was engaged in research on modeling reactors. Her current research interests include the design, fabrication, and characterization of organic photovoltaic cells.

Russell J. Holmes (M'05) received the B.Sc. (Honors) degree in physics from the University of Manitoba, Winnipeg, MB, Canada, in 2000, and the M.A. and Ph.D. degrees in electrical engineering from Princeton University, Princeton, NJ, in 2002 and 2006, respectively.

Since 2006, he has been with the faculty of the Department of Chemical Engineering and Materials Science at the University of Minnesota, Minneapolis. His current research interests include fundamental optoelectronic properties of organic and hybrid organic–inorganic materials and their application in light-emitting devices, photovoltaic cells, and lasers.